

Reinforcement of polypropylene with lignocellulose nanofibrils and compatibilization with biobased polymers

Ana Ferrer,¹ Ingrid C. Hoeger,¹ Xiaomin Lu,¹ Orlando J. Rojas^{1,2}

¹Department of Forest Biomaterials, North Carolina State University, Raleigh North Carolina

²Department of Forest Products Technology, Aalto University, Espoo 00076, Finland

Correspondence to: O. J. Rojas (E-mail: orlando.rojas@aalto.fi)

ABSTRACT: Freeze-dried and milled lignocellulose nanofibrils (LCNF) were used to reinforce polypropylene (PP) nanocomposites. The LCNF, containing up to 9% lignin, was obtained from residual Empty Palm Fruit Bunch (EPPB) fibers. Soy protein isolate (SPI) and hydroxypropyl cellulose (HPC) were tested as coupling agents as well as maleic anhydride *grafted* polypropylene (MAPP), which was used as a reference. A good level of dispersion of LCNF in the PP matrix while mechanical testing and thermal analyses indicated an improvement of the thermo-mechanical behavior of the nanocomposites was revealed upon loading of the lignin-containing nanofibrils. The tensile modulus of PP was increased by 15% upon the addition of 1% LCNF with SPI as a compatibilizer. Likewise, the thermal stability of the composites was most markedly enhanced. Overall, LCNF and SPI, two important bioresources, are introduced here for the development of novel and cost-effective PP-based composites. © 2016 Wiley Periodicals, Inc. *J. Appl. Polym. Sci.* **2016**, *133*, 43854.

KEYWORDS: cellulose and other wood products; composites; differential scanning calorimetry; extrusion; nanocellulose; thermogravimetric analysis

Received 23 July 2015; accepted 20 April 2016

DOI: 10.1002/app.43854

INTRODUCTION

The replacement of non-renewable resources by widely available and sustainable materials is a major thrust in current developments. For composites, such efforts entail the substitution of reinforcing man-made glass fibers as well as mineral particles (talc, mica, and others) with sustainable components. The intrinsic properties of nanocellulose make it ideal to reinforce high performance nanocomposites. This is because its renewability, compostability, high surface area, high specific strength, and modulus.¹ Because of its versatility, nanocelluloses can in fact enhance multiple properties of the polymer matrix or even endow the system with new functions. For example, silver nanoparticles have been attached to cationic cellulose nanocrystals (CNC) that were used to reinforce waterborne polyurethane; the resulting nanocomposites exhibited improved mechanical performance and antibacterial activity.²

The number of investigations related to cellulose in nanocomposite reinforcement, including cellulose micro/nano-fibrils (CMF and CNF) and cellulose nanocrystals (CNC), has increased rapidly in recent years. Such nanocomposites can be classified according to the polymer matrix either as hydrophilic

or nonpolar. The effective incorporation of nanocellulose in hydrophilic polymers has been demonstrated, for example, with polyvinyl alcohol,³ poly(ethylene oxide),⁴ poly(styrene-*co*-butyl acrylate),⁵ and waterborne polyurethane,² among others. Combination of nanocellulose with nonpolar polymers have included polylactic acid,⁶ polycaprolactone,⁷ polyethylene,⁸ and polypropylene (PP).^{9–12} However, the addition of nanocellulose in this latter group is a challenge, especially because of limitations in the extent of dispersion. Together with the expected poor adhesion at the phase boundaries,¹ such issues need to be addressed if high-scale production of nanocellulose-based composites is to become a reality. Physical treatments, chemical grafting and coupling agents have been used to overcome related challenges, mainly by introducing better compatibility and surface hydrophobicity onto nanocellulose.¹³ Coupling agents interact with both the matrix and the reinforcement component and facilitate their adhesion. Several proteins have been used to increase the surface energy of polyolefins¹⁴ which, for instance, could be also considered for composite manufacture. Lysozyme and fibrinectin have been shown to be effective for this purpose; however, more attractive prospects exist in the case of readily available and inexpensive proteins derived from soy beans.¹⁵ Soybean

Additional Supporting Information may be found in the online version of this article.

© 2016 Wiley Periodicals, Inc.

proteins have found industrial, nonfood applications, for example, in the manufacture of plastics, adhesives, paper binders, composites, paints, dry strength additives for papermaking, paper coatings, and sizing agents.¹⁶ We reported on the interactions of soybean proteins with both hydrophilic and hydrophobic substrates^{17,18} and studied the possibility of modifying the surface of lignin as well as hydrophobic self-assembled monolayers, both of which became hydrophilic upon soy protein adsorption. Further, a facile procedure for surface modification of polypropylene (PP) fibers via physical interactions with soy proteins was proposed.¹⁵ The effectiveness of commercial soybean isolate and flour in increasing the surface energy of PP was demonstrated.

Hydroxypropyl cellulose (HPC) belongs to the group of cellulose ethers that has been used already as glue and sizing material.¹⁹ HPC is soluble in water as well as in polar organic solvents, making it possible to combine aqueous and nonaqueous systems. HPC has been used as a topical ophthalmic protectant and lubricant, food additive, thickener and emulsion stabilizer, etc.¹⁹ Thin films of HPC, poly(vinyl alcohol) (PVA), and their blends (PVC/HPC) have been produced. Their miscibility was studied by varying the PVC/HPC ratio and the morphology and thermal stability of the respective composite films were determined.¹⁹

Maleic anhydride, one of the most commonly utilized coupling agents, has been applied to cellulose to improve its compatibility with nonpolar polymer matrices, including polyolefins. Such polymers can be used in a variety of applications taking advantage of its low price and favorable properties such as hardness, stiffness, light weight, weather, and chemical resistance and design flexibility.^{10,20} Polypropylene composites are usually reinforced with glass fibers, talc, mica minerals but also with natural fibers.^{21,22} The properties of cellulose nanofibrils (CNF) make them an attractive reinforcement component. Mostly, the reported composites include cellulose nanofibrils^{10,11} and maleic anhydride *grafted* polypropylene (MAPP) as a coupling agent.^{12,23} Suzuki *et al.* (2013), reported an improved tensile modulus and strength, twice and 1.5 times as high compared to neat PP, respectively, for PP nanocomposites loaded with CMF (50 wt %) and MAPP (5.6 wt %). Likewise, Peng *et al.* (2014) reported property enhancements (by 36% in tensile modulus, 11% in strength, 21% in flexural modulus, 7% in flexural strength and 23% in impact strength) of PP nanocomposites that included CNF (6 wt %) and MAPP (2 wt %). Fracture analysis was used to explain this significant increase in mechanical performance. The results demonstrate that the size of CNF leads to a large interfacial area and has a positive effect in the structure of the composites, which requires a large energy to initiate fracture and dissipate the energy at the interface, thereby effecting crack propagation.²⁴ Furthermore, Suzuki *et al.* (2013) showed that lignocellulosic microfibrils were able to positively impact the mechanical properties of PP. The hydrophobic nature of residual lignin relative to that of cellulose is expected to impart good compatibility between lignocellulose microfibrils and PP.¹²

With regards to the manufacture, it has been noted that the presence of water in the compounding process has a negative

impact on cellulose since it can promote substantial degradation.¹ This is most relevant to CNF, which is usually available as an aqueous dispersion. Indeed, the high moisture absorption of natural fibers/fibrils leads to swelling and can produce interfacial voids in composites, which result in poor mechanical properties and dimensional stability.²⁵ In sum, when nanocellulose fibrils are used in composites, the absorption of water by the fibrils severely degrades the properties of the composites.²⁶ This presents a problem when using CNF in composites where it also aggregates upon drying.²⁷ The different methods to dry CNF for incorporation in PP nanocomposites have shown a great impact on the mechanical properties of the resulting materials.⁹ The degree of crystallinity and morphology of the CNF reinforcing phase play a prominent role in the macroscopic properties exhibited by the composites.²⁸ Moreover, in the extrusion of plastic composites reinforced with lignocellulosic fibers, the compounding temperature is commonly restricted to about 200 °C; this is because lignocellulosic materials start to degrade at ~230 °C.²⁹ The elastic modulus, tensile strength, drawing behavior, permeability to vapors, electrical, and optical properties of the matrix are directly related to its crystalline microstructure. In turn, the crystallinity depends on the crystallization temperature (T_c), cooling rate, nucleation density, and annealing time. Overall, physical properties such as degree of crystallinity, spherulite size, lamella thickness, and crystallite orientation have a profound effect on the ultimate properties of the polymer matrix, and thus the composite.²⁸ In turn, the Young's modulus of cellulose depends on its crystallinity and the interaction of amorphous and crystalline regions. As a result, highly crystalline nanocellulose may result in potentially high mechanical properties in reinforced composites, according to the rule of mixtures. However, the water holding capacity of nanocellulose can drastically degrade the properties of the composites.²⁹

In this work, we use lignocellulose nanofibrils (LCNF), with lignin content of up to 9%, as reinforcement component in PP-based nanocomposites. Three different coupling agents or compatibilizers were evaluated, namely, soy protein isolate (SPI), hydroxypropyl cellulose (HPC), as well as maleic anhydride *grafted* polypropylene (MAPP), which was used as a reference. Freeze-milling of the dried LCNF was used to overcome aggregation. The dispersion of LCNF and the thermal and mechanical properties of the LCNF-PP nanocomposites in the presence of the compatibilizers were evaluated.

EXPERIMENTAL

Materials

The isotactic polypropylene (PP) used as thermoplastic matrix polymer was supplied by M. Holland (Braskem PP CP360CH) in the form of impact-modified homopolymer pellets with a melt flow index of 34 g·10 min⁻¹ (230 °C/2.16 kg). PP was ground into powder form using 6750 freezer/mill from SPEX CertiPrep. These samples were ground for five cycles. In each cycle, the samples were precooled by liquid nitrogen for 2 min, and then ground for 5 min. Lignocellulose nanofibrils (LCNF) were obtained from Empty Palm Fruit Bunch (EPFB) fibers from a Malaysian oil palm mill and supplied by Straw Pulping

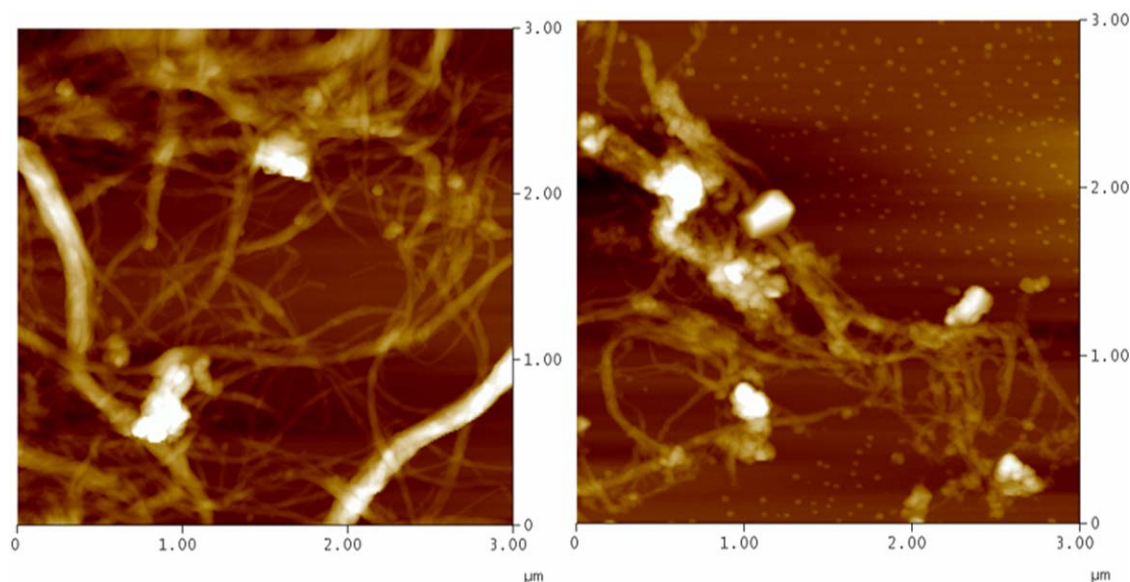


Figure 1. Height AFM images ($3\ \mu\text{m} \times 3\ \mu\text{m}$) of LCNF before (left) and after (right) freeze-milling. [Color figure can be viewed in the online issue, which is available at wileyonlinelibrary.com.]

Engineering S.L. (Zaragoza, Spain). The chemical composition of the EPFB fibers as well as the LCNF isolation are described in the Supporting Information. The LCNF chemical composition was determined by using standard methods used for EPFB fibers (described in Supporting Information) and indicated 80% holo-cellulose, 74% α -cellulose, 9% lignin, 8% extractives, and 1% ash. The additives used in order to improve the compatibility of LCNF with the thermoplastic matrix included soy protein isolate, SPI, used in powdered form (ClarisonTM 100; code 066100; lot number 13060291), hydroxypropyl cellulose, HPC ($M_w = 100,000$; Sigma-Aldrich) and maleic anhydride *grafted* polypropylene, MAPP ($M_w = 9,100$; 8–10% maleic anhydride; Sigma-Aldrich). Prior to the compounding LCNF was freeze dried (Labconco Freezezone 2.5). The sample was equilibrated at $-85\ ^\circ\text{C}$ for at least 3 h, after which it was dried at the same temperature by reducing the pressure and using a condenser temperature of $-85\ ^\circ\text{C}$. Afterward, the dried LCNF was ground into powder form using 6750 Freezer/mill from SPEX CertiPrep and ground for five cycles. In each cycle, the samples were pre-cooled by liquid nitrogen for 2 min, and then ground for 5 min. Atomic force microscopy (Dimension 3000 scanning probe Veeco Metrology Group) was used to evaluate the changes in morphology of the LCNF before and after freeze-milling (Figure 1). No apparent erosion or degradation of the fibrils was observed.

Compounding and Composite Preparation

PP was blended with the LCNF and/or compatibilizers in a co-rotating twin $15\ \text{cm}^3$ screw using melt blending and extrusion (DSM Xplore, Netherlands). The temperature of the mixing zone in the barrel was maintained at $180\ ^\circ\text{C}$ with a screw speed of 100 rpm and the mixture was blended for 3 min. Extruded blend samples were stored in sealed polyethylene bags to avoid moisture infiltration. The LCNF loading in PP was 1 and 3 wt % based on the total weight of the composite. The three types of coupling agents or compatibilizers (HPC, MAPP or SPI) were applied at 10 wt % based on the total weight of

LCNF. Freeze-dried and milled LCNF was immersed in MAPP solution (5 wt %) in toluene at $180\ ^\circ\text{C}$, equilibrated for 5 min and the solvent was evaporated before blending with PP in the extruder. In the case of SPI, aqueous dispersions of LCNF (1 wt %) and SPI were mixed and heated at $85\ ^\circ\text{C}$ for 30 min under stirring, then the mixture was dried using freeze-drying and freeze-milled following the same procedure explained above before blending with PP in the extruder. In the case of the HPC, the LCNF was freeze-dried and milled before blending with HPC and PP in the extruder. Films from the extruded samples were prepared by hot pressing in an electrically-heated press operated at $180\ ^\circ\text{C}$ for 3 min using a force of 44 kN and a pressure of 1.40 kPa. Under these conditions, the diameter and thickness of the composite films were about $20 \pm 2\ \text{cm}$ and $160 \pm 20\ \mu\text{m}$, respectively. After press molding, the samples were cooled at room temperature under pressure.

Composite Thermal and Physical Properties

XRD analysis of the LCNF before and after freeze-milling were carried out by wide-angle X-ray diffraction (Rigaku-D/MAX instrument) operating at 40 kV/44 mA with a Cu $K\alpha$ radiation (wavelength, $\lambda = 0.154\ \text{nm}$). The samples were laid on the glass sample holder and scanned at $0.6\ \text{deg}/\text{min}$ under the 2θ diffraction angle ranging from 5° to 40° . The X-ray apparent crystallinity or crystallinity index (CI, %) of cellulose was determined from the intensity ratio between the crystalline peak and the total intensity after carrying out background signal subtraction (corresponding to non-crystalline phase), according to the following equation [eq. (1)]³⁰:

$$\text{CI}(\%) = 100 \times \frac{I_{002} - I_{\text{non-cr}}}{I_{002}} \quad (1)$$

I_{002} refers to the peak maximum intensity assigned to the sample plane with the 002 Miller indices at a 2θ angle between $22\text{--}24^\circ$ and $I_{\text{non-cr}}$ is referred to the non-crystalline diffraction intensity of the material, which is measured at $2\theta = 18^\circ$, in the

valley between the 002 and 101 peaks. Scanning electron microscopy was used to observe the microstructure and the transversal morphology of PP composite films (Supporting Information). Cross sections of fractured composites (liquid nitrogen) were imaged with a Hitachi S 3200 N SEM operating at 5 kV and a working distance of 20 mm. Density values of the composites were calculated using the apparent thickness and measured mass per unit area. The composite thickness was determined using TAPPI Method T411 by means of a Lorentzen and Wettre Micrometer 51 instrument. The mass per unit area was determined using TAPPI standard T410. The degree of crystallinity (mass fraction, $W_{c,d}$) based on density (ρ) was calculated using [eq. (2)]²²:

$$W_{c,d} = \frac{1/\rho_s - 1/\rho_a}{1/\rho_c - 1/\rho_a} \times 100 \quad (2)$$

where ρ_s , ρ_c , and ρ_a stand for the density of the sample, completely crystalline (0.95 g cm⁻³) and completely amorphous (0.86 g cm⁻³) polypropylene, respectively.

Thermogravimetric analyses (TGA) were carried out with a TA instruments TGA Q-500. Samples (~10 mg) were equilibrated at 80 °C for 5 min to remove water and then heated from 80 to 800 °C at a heating rate of 10 °C min⁻¹ under flowing nitrogen (60 mL min⁻¹). DSC analyses of neat PP, SPI, HPC, MAPP, and PP blends were carried out using a TA Instrument DSC Q100 with 5–8 mg of each composite under flowing nitrogen. Each sample was scanned from 40 to 225 °C at a heating rate of 10 °C min⁻¹ to eliminate the thermal history and then cooled at the same rate and reheated under the same conditions. The melting (T_m) and crystallization (T_c) temperatures, in addition to the associated enthalpy change in each process were determined. Universal tensile tests were carried out at 23 °C and 50% relative humidity (RH) following EN ISO 291:2008 standard using an Instron 4443 Vertical Tensile Tester equipped with a 490 N load cell. Strips 5 mm in width and 40 mm in length were stamped out from composite films according to ISO 527, using a laser cutting die. The tests were performed with a cross-head speed of 2.54 mm min⁻¹. Tensile index, the tensile strength divided by the weight per unit area as well as the average and standard deviation of eight measurements were reported.

Chemical Analyses

FTIR analyses of LCNF (before and after freeze-milling) and also of PP, SPI, HPC, MAPP, and PP blend samples were carried out in order to identify characteristic bands related to amorphous and crystalline phases, as well as band displacement and/or widening as a result of the interactions between the components in the blend (Supporting Information). The analyses were performed in a PerkinElmer FTIR spectrometer Frontier equipment, in the transmission mode, from 4000 to 650 cm⁻¹ at a resolution of 4 cm⁻¹. The spectra were normalized with zero point at 670 cm⁻¹ and ordinate limit at 1.5 A.U.

RESULTS AND DISCUSSION

Thermal Behavior

The TG and DTG profiles of neat PP, LCNF, SPI, HPC, and MAPP are shown in Figure 2, which also includes the profiles

corresponding to PP and those of composites with 1 and 3% LCNF. In addition, Table I includes the value of the onset temperature of degradation T_{onset} , defined here as the temperature at which the weight loss is 5%.

The volatilization of PP in a single step takes place at 340 °C with a maximum rate at 405 °C. The mass loss of neat PP occurs very slowly at temperatures below 357 °C, which is the onset of thermal degradation, but above this temperature the process takes place very rapidly. The thermal degradation of PP occurs via random chain scission and by radical formation.¹⁰ The major source of thermal degradation in LCNF is the degradation of the cellulose component.³¹ According to Figure 2 (top panel), the degradation of LCNF occurs in two stages. In the range of (280–300 °C), a first mass loss takes place, attributed to the decomposition of hemicellulose and cellulose. The second mass loss (360–400 °C) is most likely assigned to the decomposition of the other components present in the LCNF, such as extractives, lignin, and others. This behavior is in agreement with other reports.^{32,33} The DTG curves in Figure 2 (top panel) prove that the thermal stability of LCNF is lower than that of neat PP in terms of maximum thermal degradation temperature (DTG peak temperature) and onset of thermal degradation. As shown in Table I, as the LCNF loading increased from 1 to 3%, the onset temperature of thermal degradation of the composite increased slightly. The onset of thermal degradation towards higher temperatures compared to PP can be explained by residual cell wall components, different than cellulose and lignin, present in the LCNF fibrils. The results do not follow simple mixing rules, as found by Yang *et al.* (2013).²¹ Instead, they can be explained by the increase of the residual mass content with cellulose loading.³¹ In the case of 1% LCNF loading T_{onset} was further increased by the addition of compatibilizer to the system (Figure 2 (middle panel) and Table I). This improvement in thermal stability can be the result of the stronger interfacial adhesion between LCNF and PP in the presence of compatibilizer.³⁴ The 3% LCNF systems presented similar T_{onset} values than that of 1% LCNF systems (Figure 2, bottom panel and Table I).

Figure 2 (middle and bottom panels) with DTG profiles indicate only one maximum thermal degradation temperature for PP. The DTG curves of PP-LCNF composites (without compatibilizer) were bimodal, with two DTG peak temperatures, which confirms the presence of both the LCNF and the PP matrix polymer.³⁵ However, when compatibilizer was added, the DTG curves became unimodal (similar to that for neat PP), which can be taken as indicative of dispersion and interfacial interaction between the components, leading to the observed improvement in thermal stability. This trend was not observed in systems with 3% of LCNF and HPC. In view of these results (Figure 2 and Table I), it is apparent that among all compatibilizer tested, SPI was the most effective at LCNF loading of 1%.

DSC Profile and Crystallinity

Thermograms of neat PP, SPI, HPC, and MAPP in the temperature range from 40 °C up to 225 °C are shown in Figure S3 (Supporting Information). The degree of crystallinity, temperature and heat of fusion (ΔH , J g⁻¹) associated with each

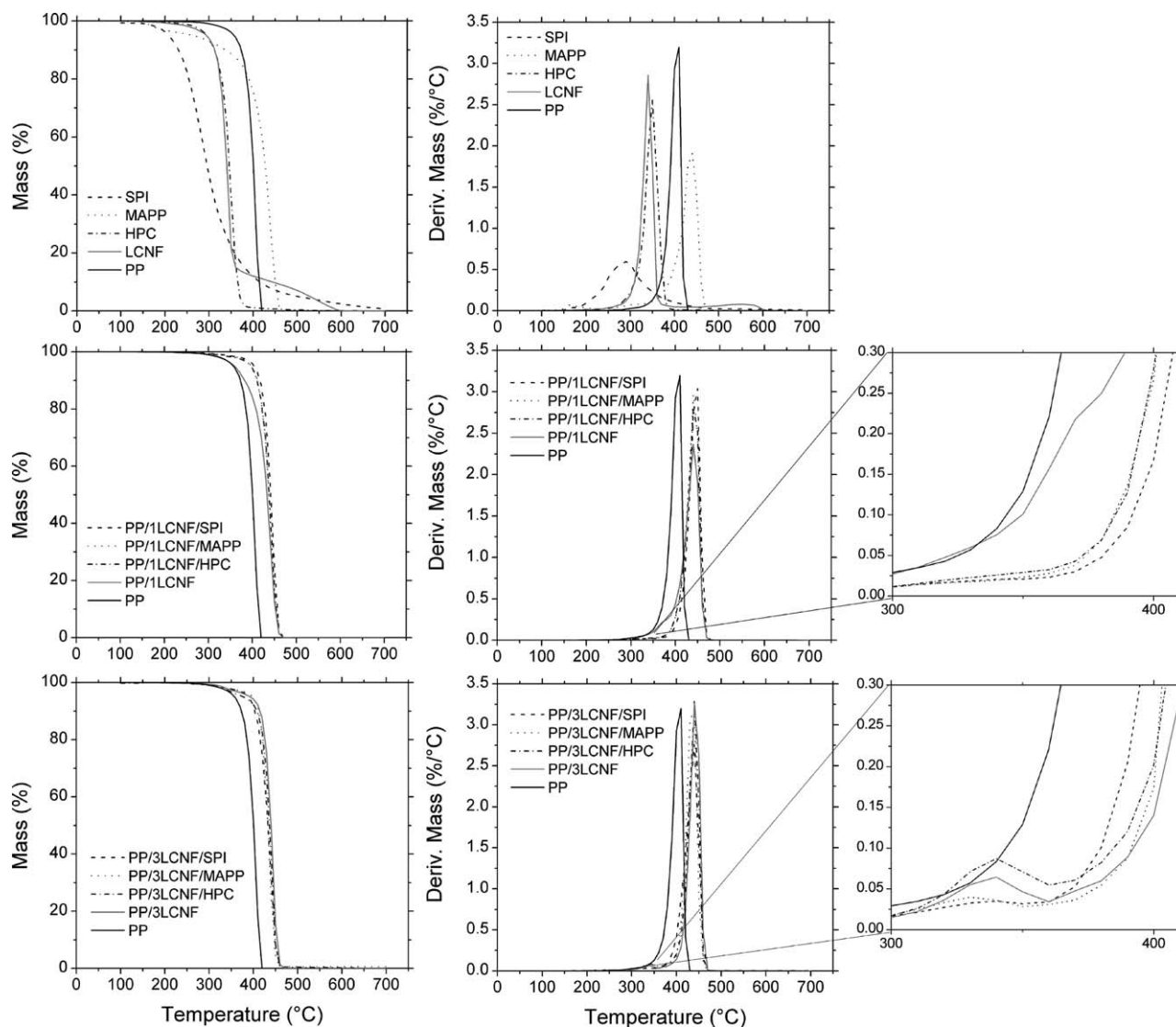


Figure 2. Top panel: TG and DTG curves of neat PP, LCNF, HPC, MAPP, and SPI in the temperature range from 100 °C to 800 °C. Middle and bottom panels correspond to the TG and DTG profiles of neat PP, and the PP-based composites with 1% and 3% LCNF loading, respectively. SPI, HPC, or MAPP are indicated as the compatibilizers used. Magnified views of some of the thermograms are also included. The initial mass loss for LCNF due to evaporation of the absorbed moisture was not recorded.

transition obtained from DSC thermograms for blend samples are summarized in Table II.

The transition temperatures (T_c and T_m) were determined in the second heating cycle (to eliminate the thermal history of the films), while the enthalpies used to calculate the degree of crystallinity were obtained in the first heating cycle in accordance to Conti *et al.* (2006).³⁶ The degree of crystallinity \bar{X}_c of the composite samples was calculated by [eq. (3)],³⁴ where $\Delta H_f(T_m)$ is the melting enthalpy of the blend during the first DSC heating cycle (J g^{-1}) and $\Delta H_f^0(T_m^0)$ is the melting enthalpy for PP 100% crystalline (138 J g^{-1}); w is the mass fraction for polymer in the composites.

$$\bar{X}_c = \frac{\Delta H_f(T_m)}{\Delta H_f^0(T_m^0)w} \times 100 \quad (3)$$

Figure 3 includes DSC curves for PP-based composites with 1 and 3% LCNF and compatibilizer (SPI, HPC, MAPP) in the

crystallization and melting transition zones. The thermal transition of PP varies with LCNF loading and with the presence of SPI, HPC and MAPP. The most important aspect is whether the resulting composites are compatible or not.¹⁹ The DSC thermograms of all composites (Figure 3) include one single broad crystallization transition peak (T_c) that increases with LCNF and compatibilizer content. The values of T_c obtained in the composites are close to that of the PP homopolymer indicating the compatibility between the components of the system. In addition, the width of thermogram around the T_c for the composites is almost identical to that of pure PP, which supports good compatibility.¹⁹ As can be observed in Figure 3 and Table II, the addition of LCNF to the PP matrix results in an increase in X_c and T_c . This can be explained by the nucleating ability of the surface of lignocellulosic nanofibrils during the crystallization and the partial crystalline growth of PP.²⁷ X_c and T_c further increased upon addition of the compatibilizer in composites

Table I. T_{onset} and DTG of Composites with PP and LCNF/(HPC/MAPP/SPI)

Composite PP/LCNF/HPC/ MAPP/SPI (wt %)	T_{onset} (°C)	DTG (°C)
100% PP	357	407
1% LCNF	360	410
1% LCNF / 10% SPI	405	455
1% LCNF / 10% HPC	397	447
1% LCNF / 10% MAPP	399	449
3% LCNF	393	443
3% LCNF / 10% SPI	389	439
3% LCNF / 10% HPC	377	427
3% LCNF / 10% MAPP	399	449

The % LCNF is based on the PP mass while that for SPI, HPC and MAPP are relative to the LCNF mass.

with 1% of LCNF. This is a clear indication of the enhanced interactions between the fibrils and PP matrix.²⁷ However, this trend was not observed in the case of the composites with 3% LCNF.

The enthalpy of crystallization (ΔH_c) of the PP phase increased with the addition of LCNF, indicating that fibrils promoted the crystallization process. Similar results were found by Joseph *et al.* (2003).²⁷ The heat of crystallization of PP was further increased by the addition of SPI and MAPP (system with 1% of LCNF, Figure 3 and Table II), which further favored the crystallization process. In the case of LCNF loading at 3% (Figure 3 and Table II), the heat of crystallization was increased only when HPC was used. Differences in shape and area of the melting endotherm peak were noticed. The data in Table II indicate that the melting points (T_m) for the composite samples were nearly around the value of PP. The introduction of LCNF with or without compatibilizer produced an increase in the PP melting peak, indicating an improvement in crystallite size, as can

be confirmed by the results related to the degree of crystallinity (see Figure 3 and Table II). The variations in shape and area are attributed to the different degrees of crystallinity found in the samples with different compatibilizer and LCNF concentrations.¹⁹ The increase in heat of fusion and T_m suggests that the crystallinity and uniformity of the crystal structure were improved with the increased compatibility between the components of the PP-based composites.

Chemical Analyses

Figure 4(a) shows FTIR spectra of LCNF before and after freeze-milling. The collected spectra display the characteristic bands attributed to cellulose. The bands around 3496 cm^{-1} (O—H), 1110 cm^{-1} (C—O of secondary alcohol) and 2868 and 2970 cm^{-1} (C—H from $-\text{CH}_2-$) were clearly identified.³⁷ More importantly, there were no significant differences between the spectra. The crystallinity index (CI, %) for the LCNF upon freeze-milling was reduced only to a limited extent (69.3 ± 2.1 and 64.1 ± 3.1 before and freeze-milling, respectively). Therefore, no significant variation in crystallinity occurred despite the observed change in the nanoscale dimension after milling. Figure 4(b,c) shows the FTIR spectra of the composite samples with 1% and 3% LCNF and SPI, HPC, and MAPP. All the spectra display similar features, typical of the PP spectrum. No changes in functional group bands were observed. 1 and 3% of LCNF loading did not cause significant changes in the molecular structure of PP. The crystallinity index or degree of crystallinity was also determined with FTIR spectra applying Lambert and Beer's law to selected peaks³⁸:

$$X_c = \frac{a_r A_{cr}}{a_{cr} A_r} \quad (4)$$

The calculation used the absorbance measurements (A_{cr} and A_r or A_{am}) (plots not shown), and the absorption coefficients (a_{cr}/a_{am} or a_r/a_{cr}) which were taken from the literature. A a_r/a_{cr} ratio of 0.79 was selected for the PP used in this study (isotactic). The crystalline nature of the absorbance peak located at

Table II. Values of Transition Temperatures, Associated Heat of Fusion and Degree of Crystallinity (\bar{X}_c) for PP/LCNF/HPC/MAPP/SPI Composites

Composite PP/LCNF/HPC/ MAPP/SPI (wt %)	At crystallization transition (T_c)				At melting phase transition (T_m)				
	T_c (°C)	ΔT_c (%)	ΔH_c (J g^{-1})	% change ΔH^a	T_m (°C)	ΔT_m (%)	ΔH_m (J g^{-1})	% change ΔH^a	\bar{X}_c (%)
100% PP	114.3	–	–103.5	–	163.0	–	81.8	–	59
99%PP/1%LCNF	115.7	1.2	–86.6	–16.4	164.3	0.8	86.4	5.6	63
98.9%PP/1%LCNF/10%SPI	119.2	4.4	–79.6	–23.1	166.9	2.4	90.6	10.8	66
98.9%PP/1%LCNF/10%HPC	117.5	2.8	–101.3	–2.1	167.2	2.6	106.6	30.3	78
98.9%PP/1%LCNF/10%MAPP	116.6	2.1	–81.2	–21.5	167.6	2.8	89.7	9.7	66
97%PP/3%LCNF	124.0	8.5	–85.1	–17.8	163.7	0.4	102.9	25.8	77
96.7%PP/3%LCNF/10%SPI	122.1	6.8	–89.4	–13.6	164.6	1	93.6	14.4	70
96.7%PP/3%LCNF/10%HPC	121.5	6.3	–80.7	–22.1	163.2	0.1	102.3	25.0	77
96.7%PP/3%LCNF/10%MAPP	121.0	5.9	–90.3	–12.8	163.4	0.3	100.1	22.3	75

$$^a \text{ \% change of } \Delta H = \frac{(\Delta H)_{\text{composite}} - (\Delta H)_{\text{pure PP}}}{(\Delta H)_{\text{pure PP}}} \times 100.$$

$$\Delta T_c = \frac{(T_c)_{\text{composite}} - (T_c)_{\text{pure PP}}}{(T_c)_{\text{pure PP}}} \times 100.$$

$$\Delta T_m = \frac{(T_m)_{\text{composite}} - (T_m)_{\text{pure PP}}}{(T_m)_{\text{pure PP}}} \times 100.$$

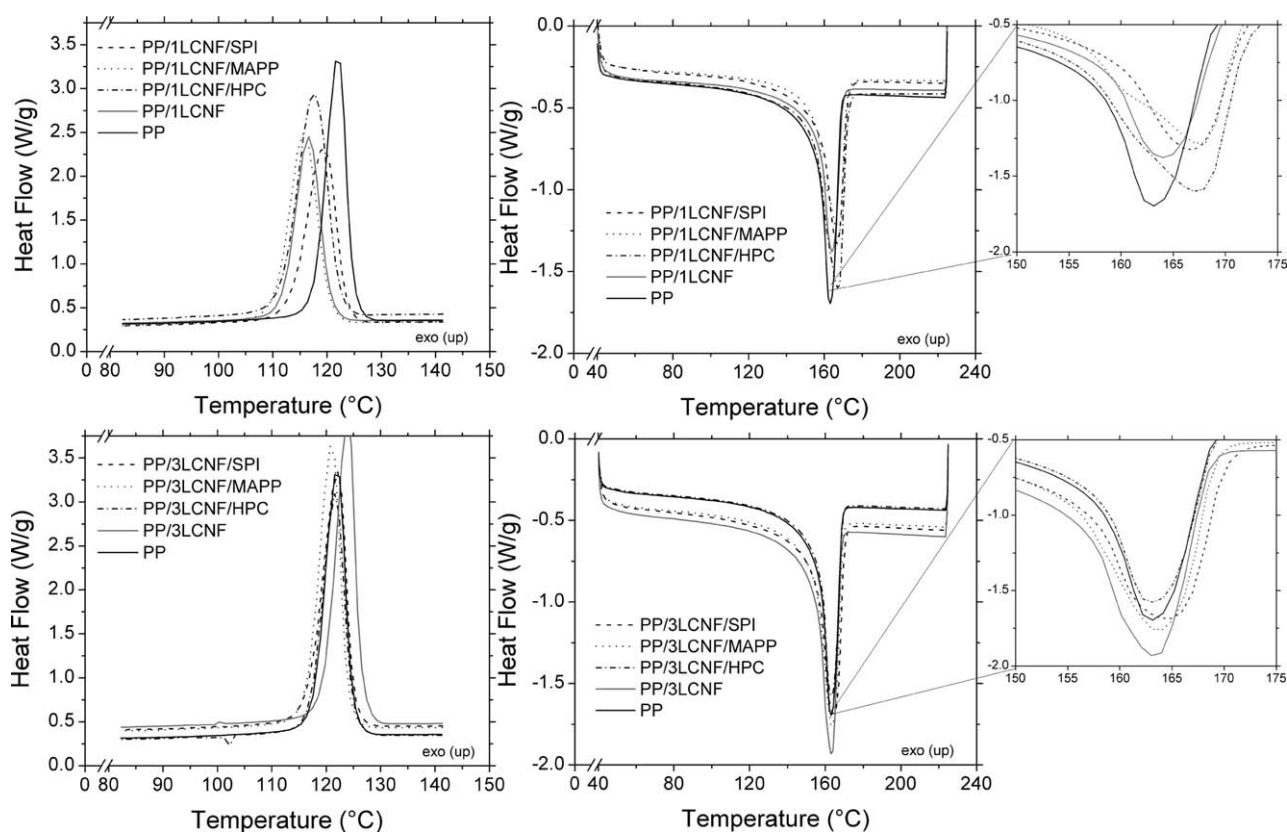


Figure 3. DSC curves of PP-based composites with 1% and 3% LCNF loading (top and bottom panels, respectively) and compatibilizer (SPI, HPC or MAPP) in the crystallization (left) and melting transitions (middle). Magnified regions of the DSC profiles are included on the right.

841 cm^{-1} was easily identified and is well referenced in the literature ($A_{cr}=A_{841}$).^{39–41} The absorbance peak at 1153 cm^{-1} was assigned to the amorphous phase content ($A_{am}=A_{1153}$).⁴⁰ Tadokoro and coworkers reported 973 cm^{-1} absorbance peak as an internal standard; as a consequence, its height should be essentially insensitive to structure, that is, to the amorphous/crystalline ratio ($A_r=A_{973}$).³⁸ Table III shows the values of the degree of crystallinity (%) for the composites calculated by FTIR. Figure 5 includes the degree of crystallinity for the composites, measured by the different techniques. As can be observed in Figure 5, the values obtained with the different methods showed

the same trend that was previously discussed with the DSC results.

Mechanical Strength

The mechanical properties of PP and PP-based composites are presented in Table IV. The PP matrix has a tensile index of 168 kN g^{-1} . A reduction in tensile index was observed when LCNF was incorporated to the polymer. Table IV shows a decrease in reinforcement efficiency as the nanofiber content increased. The addition of LCNF did not improve the strength, which could be an indication of insufficient adhesion between the fibrils and

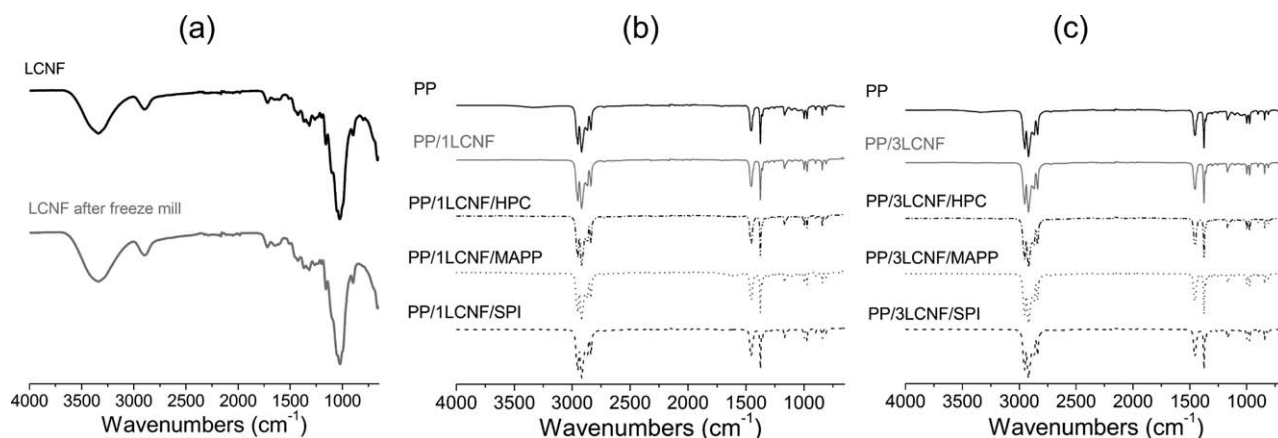


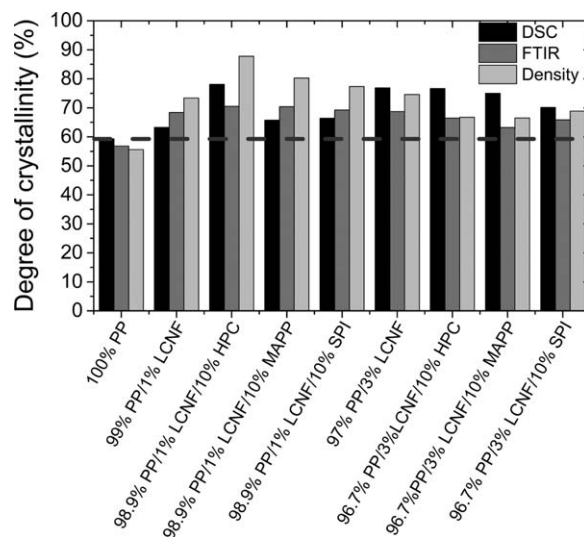
Figure 4. FTIR spectra of LCNF before and after freeze-milling (a); neat PP and the PP-based composites with 1% (b) and 3% (c) LCNF with and without compatibilizer (SPI, HPC or MAPP).

Table III. Values of the Degree of Crystallinity (%) for PP/LCNF/HPC/MAPP/SPI Composites Calculated by FTIR

PP/LCNF/HPC/MAPP/SPI (wt %)	Degree of crystallinity (FTIR) (%)	Degree of crystallinity (density) (%)
100% PP	57	56
99% PP / 1% LCNF	68	73
98.9% PP / 1% LCNF / 10% SPI	69	77
98.9% PP / 1% LCNF / 10% HPC	71	88
98.9% PP / 1% LCNF / 10% MAPP	70	80
97% PP / 3% LCNF	69	75
96.7% PP / 3% LCNF / 10% SPI	66	69
96.7% PP / 3% LCNF / 10% HPC	67	67
96.7% PP / 3% LCNF / 10% MAPP	63	67

The values obtained from density data [eq. (2)] are also included as a reference.

the matrix and that the stress cannot be transferred from the matrix to the stronger fibrils.^{42,43} At high deformations, as in tensile tests, the absence of good adhesion at the interface reduces the strength.⁴⁴ In the presence of the compatibilizer (SPI or MAPP), the tensile index was increased (ca. 8% in the case of 1% LCNF loading and 10% MAPP), which highlights an improved interfacial bonding between cellulose and PP.⁴⁵ In fact, several studies have shown the important effect of MAPP on the mechanical properties of fiber-reinforced composites.^{42,46,47} From the results, the effectiveness of SPI and MAPP as compatibilizer is clearly observed. The addition of 10 wt % of MAPP to the composite with 1% LCNF increased the tensile index by about 12% compared to the same composite in the absence of compatibilizer. The presence of 10 wt % MAPP was probably not enough to act as a coupling agent with 3%

**Figure 5.** Values for the degree of crystallinity calculated by using different methods (DSC, FTIR, and density). The horizontal dotted line corresponds to the crystallinity of neat PP and is added as a reference.

LCNF⁴⁸ and, probably, the same logic could be applied to the case of HPC.

An important improvement in the tensile index was observed when SPI was added as compatibilizer in the system with 3% LCNF. The hydroxyl groups of LCNF interact with amino and acid groups in the protein, thus decreasing inter- and intramolecular interactions between protein chains, and thus improving its motion ability, which results in better flexibility.⁴⁹

As indicated in Table IV, the relative tensile modulus increased for LCNF loading of 1%; unexpectedly, it decreased slightly at 3% LCNF loading. Besides the contribution of stiff fillers, the increase of relative tensile modulus in PP composites in the absence of the compatibilizer indicates an increase in the rigidity of PP because of the restrictions of macromolecules mobility and deformability imposed by the filler.⁴⁵ The presence of the compatibilizer improves the interaction of LCNF with the matrix, enhancing stress transfer. However, as can be seen in

Table IV. Mechanical Properties of PP/LCNF/(HPC/MAPP/SPI) Composites

Composite	Elongation at break (%)	Max. load (N)	Tensile index (kN g ⁻¹)	Tensile strength (MPa)	Tensile modulus (kN g ⁻¹)	Tensile modulus (MPa)
100% PP	5.3 ± 0.2	16.7 ± 2.0	168 ± 22	22 ± 3	8695 ± 469	1113 ± 60
1% LCNF	5.5 ± 0.9	17.8 ± 2.0	162 ± 15	20 ± 2	9803 ± 336	1196 ± 41
1% LCNF / 10% SPI	4.9 ± 0.3	17.5 ± 2.0	173 ± 15	20 ± 2	11,034 ± 759	1280 ± 88
1% LCNF / 10% HPC	4.0 ± 0.9	20.1 ± 2.9	164 ± 26	20 ± 3	7942 ± 760	961 ± 92
1% LCNF / 10% MAPP	7.1 ± 1.0	19.2 ± 2.9	181 ± 15	22 ± 2	10,388 ± 298	1257 ± 36
3% LCNF	5.7 ± 0.3	19.5 ± 2.0	161 ± 17	20 ± 2	9573 ± 710	1187 ± 88
3% LCNF / 10% SPI	6.4 ± 1.3	17.3 ± 2.9	205 ± 35	19 ± 3	12,217 ± 924	1124 ± 85
3% LCNF / 10% HPC	4.5 ± 0.3	17.7 ± 1.0	161 ± 18	18 ± 2	10,607 ± 554	1188 ± 62
3% LCNF / 10% MAPP	4.5 ± 0.3	15.8 ± 2.0	135 ± 14	18 ± 2	8903 ± 313	1193 ± 42

The % LCNF is based on the PP mass while that for SPI, HPC, and MAPP are relative to the LCNF mass.

Table IV, HPC and MAPP were of no benefit in the systems with 1 and 3% LCNF, respectively, since the modulus values were lower compared to the ones shown for the composite formulations without compatibilizer.

No statistically significant differences could be observed for the maximum load values. LCNF did not have a significant effect on the elongation at break (%) except for the sample with 1% LCNF and MAPP, which showed a higher value (ca. 7%). In general, the highest LCNF concentration did not increase or improve the mechanical properties significantly. The reason for this can be nanofiber agglomeration at high LCNF loading, as dispersion of nanosized reinforcement in the matrix polymer is the main challenge in melt compounding of nanocomposites.^{42,50} Alternatively, LCNF degradation could be a factor. SPI addition showed a remarkable effect in terms of mechanical properties.

CONCLUSIONS

Composite films of PP reinforced with LCNF were successfully produced by extrusion after freeze-milling of LCNF to induce nanofibrils dispersion. This allowed the use of dry LCNF for compounding in the PP matrix. SPI, HPC, and MAPP improved the compatibility between LCNF and the PP matrix, as indicated by the increased degree of crystallinity and enhanced thermal properties of the respective composites. Based on the results obtained in this study, the thermal stability of the composites was improved by using biobased, inexpensive and widely available soy protein isolate (SPI) as well as HPC and MAPP.

ACKNOWLEDGMENTS

The authors of this work are grateful to Spain's DGICYT for funding this research within the framework of the Projects TRA2009-0064 and CTQ2010-19844-C02-01. Dr. Carlos Salas is also acknowledged for his support.

REFERENCES

- Hubbe, M. A.; Rojas, O. J.; Lucia, L. A.; Sain, M. *BioResources* **2008**, *3*, 929.
- Liu, H.; Song, J.; Shang, S.; Song, Z.; Wang, D. *ACS Appl. Mater. Interfaces* **2012**, *4*, 2413.
- Zimmerman, T.; Poehler, E.; Geiger, T. *Adv. Eng. Mater.* **2004**, *6*, 754.
- Azizi Samir, M. A. S.; Alloin, F.; Sanchez, J. Y.; Dufresne, A. *Polymer* **2004**, *45*, 4149.
- Favier, V.; Canova, G. R.; Cavaille, J. Y.; Chanzy, H.; Dufresne, A.; Gauthier, C. *Polym. Adv. Technol.* **1995**, *6*, 351.
- Stoeffler, K.; Ton-That, M. T.; Denault, J.; Luong, J.; Wu, C.; Sain, M. *68th Annu. Tech. Conf. Soc. Plast. Eng.* **2010**, 223.
- Mathew, A. P.; Oksman, K.; Sain, M. *J. Appl. Polym. Sci.* **2005**, *97*, 2014.
- Panaiteescu, D. M.; Notingher, P. V.; Ghiurea, M.; Ciuprina, F.; Paven, H.; Iorga, M.; Florea, D. *J. Optoelectron. Adv. Mater.* **2007**, *9*, 2524.
- Khoshkava, V.; Kamal, M. R. *ACS Appl. Mater. Interfaces* **2014**, *6*, 8146.
- Yang, H. S.; Kiziltas, A.; Gardner, D. J. *J. Therm. Anal. Calorim.* **2013**, *113*, 673.
- Yang, H. S.; Gardner, D. J.; Nader, J. W. *J. Therm. Anal. Calorim.* **2011**, *103*, 1007.
- Suzuki, K.; Okumura, H.; Kitagawa, K.; Sato, S.; Nakagaito, A. N.; Yano, H. *Cellulose* **2013**, *20*, 201.
- Abdelmouleh, M.; Boufi, S.; ben Salah, A.; Belgacem, M. N.; Gandini, A. *26th Proc. Annu. Meet. Adhes. Soc.* **2003**, 237.
- Goli, K. K.; Rojas, O. J.; Özçam, O.; Genzer, J. *Biomacromol.* **2012**, *13*, 1371.
- Salas, C.; Genzer, J.; Lucia, L. A.; Hubbe, M. A.; Rojas, O. J. *ACS Appl. Mater. Interfaces* **2013**, *5*, 6541.
- Schmitz, J. F.; Erhan, S. Z.; Sharma, B. K.; Johnson, L. A.; Myers, D. J. In *Soybeans Chemistry, Production, Processing, and Utilization*; Johnson, L. A.; White, P. J.; Gallowa, R., Eds.; American Oil Chemists' Society Press: Urbana, IL, **2008**; p 539.
- Salas, C.; Rojas, O. J.; Lucia, L. A.; Hubbe, M. A.; Genzer, J. *Biomacromolecules* **2012**, *13*, 387.
- Salas, C.; Rojas, O. J.; Lucia, L. A.; Hubbe, M. A.; Genzer, J. *ACS Appl. Mater. Interfaces* **2012**, *5*, 199.
- Guirguis, O. W.; Moselhey, M. T. *Nat. Sci.* **2012**, *4*, 57.
- Aubin, F. In *Mechanical and Materials Engineering*; University of Nebraska: Lincoln, **2013**.
- Karnani, R.; Krishnan, M.; Narayan, R. *Polym. Eng. Sci.* **1997**, *37*, 476.
- Munaro, M.; Akcelrud, L. *J. Polym. Res.* **2008**, *15*, 83.
- Peng, Y.; Gallegos, S. A.; Gardner, D. J.; Han, Y.; Cai, Z. *Polym. Compos.* **2016**, *37*, 782.
- Yang, H. S.; Gardner, D. J.; Nader, J. W. *J. Appl. Polym. Sci.* **2013**, *128*, 3064.
- John, M. J.; Thomas, S. *Carbohydr. Polym.* **2008**, *71*, 343.
- Espert, A.; Vilaplana, F.; Karlsson, S. *Compos. A* **2004**, *35*, 1267.
- Peng, Y.; Gardner, D. J.; Han, Y. *Cellulose* **2012**, *19*, 91.
- Joseph, P. V.; Joseph, K.; Thomas, S.; Pillai, C. K. S.; Prasad, V. S.; Groeninckx, G.; Sarkissova, M. *Compos. A* **2003**, *34*, 253.
- Peng, Y.; Gardner, D. J.; Han, Y.; Kiziltas, A.; Cai, Z.; Tshabalala, M. A. *Cellulose* **2013**, *20*, 2379.
- Segal, L.; Creely, J.; Martin, A.; Conrad, C. *Text. Res. J.* **1959**, *29*, 786.
- Yang, H. S.; Wolcott, M. P.; Kim, H. S.; Kim, H. J. *J. Therm. Anal. Calorim.* **2005**, *82*, 157.
- Alemdar, A.; Sain, M. *Compos. Sci. Technol.* **2008**, *68*, 557.
- Jonoobi, M.; Niska, K. O.; Harun, J.; Misra, M. *BioResources* **2009**, *4*, 626.
- Kim, H. S.; Lee, B. H.; Choi, S. W.; Kim, S.; Kim, H. J. *Compos. A* **2007**, *38*, 1473.

35. Lönnberg, H.; Fogelström, L.; Berglund, L.; Malmström, E.; Hult, A. *Eur. Polym. J.* **2008**, *44*, 2991.
36. Conti, D. S.; Yoshida, M. I.; Pezzin, S. H.; Coelho, L. A. F. *Thermochim. Acta* **2006**, *450*, 61.
37. Missoum, K.; Martoia, F.; Belgacem, M. N.; Bras, J. *Ind. Crops Prod.* **2013**, *48*, 98.
38. Lamberti, G.; Brucato, V. *J. Polym. Sci. B: Polym Phys* **2003**, *41*, 998.
39. Painter, P. C.; Watzek, M.; Koenig, J. L. *Polymer* **1977**, *18*, 1169.
40. Tadokoro, H.; Kobayashi, M.; Ukita, M.; Yasufuku, K.; Murahashi, S.; Torii, T. *J. Chem. Phys.* **1965**, *42*, 1432.
41. Ward, I. M. *Structure and Properties of Oriented Polymers*, 2nd ed.; Chapman & Hall: London, **1997**.
42. Oksman, K.; Mathew, A. P.; Långström, R.; Nyström, B.; Joseph, K. *Compos. Sci. Technol.* **2009**, *69*, 1847.
43. Thomason, J. L. *Compos. A* **2002**, *33A*, 1641.
44. Mohd. Ishak, Z. A.; Ariffin, A.; Senawi, R. *Eur. Polym. J.* **2001**, *37*, 1635.
45. Panaitescu, D. M.; Donescu, D.; Bercu, C.; Vuluga, D. M.; Iorga, M.; Ghiurea, M. *Polym. Eng. Sci.* **2007**, *47*, 1228.
46. Patankar, S. N.; Das, A.; Kranov, Y. A. *Compos. A* **2009**, *40A*, 897.
47. Vilaseca, F.; Valadez-Gonzalez, A.; Herrera-Franco, P. J.; Pèlach, M. A.; López, J. P.; Mutjé, P. *Bioresour. Technol.* **2010**, *101*, 387.
48. Hassan, A.; Abd. Rahman, N.; Yahya, R. *J. Reinf. Plast. Compos.* **2011**, *30*, 1223.
49. Guerrero, P.; Retegi, A.; Gabilondo, N.; de la Caba, K. *J. Food Eng.* **2010**, *100*, 145.
50. Oksman, K.; Mathew, A. P.; Bondeson, D.; Kvien, I. *Compos. Sci. Technol.* **2006**, *66*, 2776.